Table 1 Wall velocity gradient f''_w and correction factor β

h_w/H_e	H_e/h_e	k	f''_w	β
0.0	1.0	0.0	0.3321	1.0000
		0.6	0.4330	1.0308
		1.2	0.5143	1.0441
	3.5	0.0	0.3321	1.0000
		0.6	0.4598	1.0946
		1.2	0.5569	1.1306
	6.0	0.0	0.3321	1.0000
		0.6	0.4815	1.1462
		1.2	0.5898	1.1974
0.5	1.0	0.0	0.3321	1.0000
		0.6	0.4468	1.0636
		1.2	0.5367	1.0896
	3.5	0.0	0.3321	1.0000
		0.6	0.4944	1.1769
		1.2	0.6092	1.2367
	6.0	0.0	0.3321	1.0000
		0.6	0.5291	1.2595
		1.2	0.6594	1.3387
1.0	1.0	0.0	0.3321	1.0000
		0.4	0.4215	1.0727
		0.8	0.4935	1.1076
		1.2	0.5559	1.1285
	2.0	0.0	0.3321	1.0000
		0.4	0.4436	1.1289
		0.8	0.5278	1.1846
		1.2	0.5995	1.2171
	3.5	0.0	0.3321	1.0000
		0.4	0.4704	1.1971
		0.8	0.5675	1.2737
		1.2	0.6487	1.3169
	6.0	0.0	0.3321	1.0000
		0.4	0.5051	1.2580
		0.8	0.6172	1.3852
		1.2	0.7096	1.4406

cross-flow are contained implicitly in f''_w. Using Eq. (5), β may be obtained from these results, which are given as a function of k, wall to total temperature ratio, and local Mach number. β is the increase or decrease in skin friction coefficient (and for $Pr=1.0$, the Stanton number) that occurs on the plane of symmetry of a sharp cone in laminar flow due only to the change in the velocity and temperature gradients at the wall created by the cross-flow gradient of velocity in the plane of symmetry. The values of f''_w calculated by Reshotko are given in Table 1 as a function of k, h_w/H_e, and H_e/h_e. Using $f'_{w_0}=0.3321$ and Eq. (5), the values of the correction factor associated with the change in velocity gradient at the wall with angle of attack may be obtained, and is also contained in Table 1. Note that the effect of the wall gradient on the total correction factor K_{cf} is very significant under certain wall and edge enthalpy conditions. To neglect it by employing only the divergence effect, Eq. (1), could seriously underpredict the laminar skin friction.

The integral analysis of Brunk[3] provides numerical values of f''_w that differ by less than 1% from Reshotko's exact values. By assuming appropriate temperature and velocity profiles, and employing these in the streamwise and circumferential integral equations in the windward plane of symmetry, Brunk provided simultaneous algebraic equations for the solution of the surface velocity gradients. Although presenting numerical comparisons with Reshotko's results, Brunk did not provide an explicit solution for f''_w. By solving the simultaneous equations obtained by Brunk, we find the following equation describing the total correction factor for laminar flow on the windward plane of symmetry

$$K_{c_f}=\beta[1+k]^{1/2}=\Big[0.4811+0.2864k+\Big\{0.2693+0.7408k+0.5903k^2+k(1+1.5k)\,(0.1572\frac{H_e}{h_e}+0.4168\frac{h_w}{h_e})\Big\}^{1/2}\Big]^{1/2} \quad (8)$$

If the term containing the enthalpy ratios in Eq. (8) is neglected, the solution essentially reduces to Eq. (5) with $\beta=1.0$. The enthalpy ratios in the solution represent the effect of the coupling between the streamwise and circumferential momentum equations. When the terms which provide this coupling in the governing differential equations are dropped and the nondimensional circumferential velocity derivative and streamwise velocity are assumed equal, the solution provides only the divergence effects.

Figure 1 shows the variation of K_{cf} with angle of attack on the windward meridian of a 7.5° cone at Mach 3.1, calculated using the analytical results of Moore.[6] Using only the streamline divergence correction factor, with $\beta=1.0$, accounts for only about one half the increase in skin friction at these conditions. Including the effects of wall gradient variations brings the correction factor into agreement with Moore's calculations.

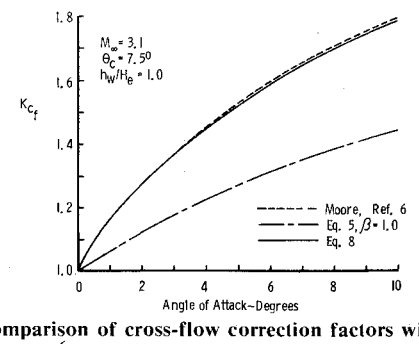

Fig. 1 Comparison of cross-flow correction factors with analytical results of Moore.[6]

References

[1] Smith, R.A. and Chang, P.K., "Compressible Laminar Boundary Layer on a Cone at High Angle of Attack," *AIAA Journal* Vol. 8, Nov. 1970, pp. 1921-1927.

[2] Reshotko, E., "Laminar Boundary Layer with Heat Transfer on a Cone at Angle of Attack in a Supersonic Stream," NACA TN 4152, Dec. 1957.

[3] Brunk, W.E., "Approximate Method for Calculation of Laminar Boundary Layer with Heat Transfer on a Cone at Large Angle of Attack in Supersonic Flow," NACA TN 4380, Sept. 1958.

[4] Adams, J.C., Jr., "Evaluation of Windward Streamline Effective Cone Boundary Layer Analyses," *Journal of Spacecraft and Rockets*, Vol. 9, Sept. 1972, pp. 718-720.

[5] Agnone, A., "Cross-Flow Effects on the Boundary Layer in a Plane of Symmetry," *Journal of Spacecraft and Rockets*, Vol. 11, July, 1974, pp. 542-544.

[6] Moore, F.K., "Laminar Boundary Layer on Cone in Supersonic Flow at Large Angle of Attack," NACA Rept. 1132, 1953.

Stability of a Gyrostat Satellite with Flexible Appendages

Robert A. Calico*
Air Force Institute of Technology, Wright Paterson Air Force Base, Ohio

Introduction

THE stability of artificial satellites with flexible appendages has received much attention in recent years. The inclusion of distributed elastic parts in modeling satellites yields a hybrid dynamical system, that is, one which is described by both ordinary and partial differential equations.

Received Dec. 19, 1975; revision received March 1, 1976.
Index categories: Spacecraft Attitude Dynamics and Control; Structural Dynamic Analysis.

*Assistant Professor, Department of Mechanics and Engineering Systems. Member AIAA.

This hybrid form precludes testing the systems stability by methods ordinarily used for discrete systems. In order to obtain a system whose stability can be readily analyzed, hybrid systems have been discretized by various methods. These include the lumped parameter method,[1,2] the assumed modes method,[3,4] and the finite element method.[5] Each of these techniques yields a set of ordinary differential equations describing the satellites motion.

A theory for the stability of a hybrid system has been developed via the use of the Liapunov direct method in Ref. 6, where it is shown that under certain circumstances the system Hamiltonian is a suitable Liapunov functional. The method of Ref. 6 works directly with the hybrid system. The system stability can also be tested by replacing the Liapunov functional by a Liapunov function by using any one of the discretization techniques mentioned above.

Another means for discretizing the system Hamiltonian is the method of integral coordinates. This technique, first introduced in Ref. 7 has the advantage of introducing only one discrete coordinate for each elastic displacement. By comparison, the lumped parameter method, the assumed modes method, and the finite-element method need many more coordinates for a reasonable stability analysis.

This Note is concerned with the application of the method of integral coordinates to the analysis of a gravity-stabilized satellite containing a number of symmetrical internal rotors. The problem formulation allows for m such rotors rigidly attached to the main body of the satellite. As an example, the stability of a satellite containing a single constant speed rotor is considered. The model considered is the same as in Ref. 8 except for the inclusion of a flexible rod attached to the main body of the satellite.

Problem Formulation and Stability Analysis

The problem formulation is essentially that of Ref. 6, except for the inclusion of the m internal rotors. The addition of the rotors give rise to new terms in the system kinetic energy of the form

$$T_R = \tfrac{1}{2}\sum_{i=1}^{m} \{\omega_i\}^T [I_{R_i}] \{\omega_i\} + \sum_{i=1}^{m} \{\Omega\}^T [\ell_{R_i}]^T [I_{R_i}] \{\omega_i\} \quad (1)$$

where $\{\Omega\}$ is the angular velocity of an axis system xyz fixed in the rigid portion of the satellite, $\{\omega_i\}$ is the angular velocity of the ith rotor relative to the axes xyz, $[\ell_R]$ is the direction cosine matrix between axes xyz and a nodal axes system for the ith rotor, and finally $[I_{R_i}]$ is the inertia matrix for the ith rotor in terms of a rotor nodal axis system. We note that the matrices $[I_{R_i}]$ are diagonal and have two equal moments of inertia. With the exception of the addition of these terms to the system kinetic energy, the formulation of Ref. 6 remains unchanged. It should be noted however that the inertia of these m rotors must be included in the inertia matrices $[J_0]$ of Ref. 6.

Our interest is in the attitude motion of a satellite whose mass center travels in a circular orbit about a planet P. It will prove convenient to define a system of orbital axes $a_1a_2a_3$, where axis a_1 coincides with the position vector to the satellites center of mass, a_2 is tangent to the orbit in the direction of the motion, and a_3 is normal to the orbit. The axes system xyz is obtained from $a_1a_2a_3$ by a 2, 1, 3 Euler angle rotation through angles $\theta_2, -\theta_1$, and θ_3, respectively. The angular velocity of the axes system xyz may now be written in the form

$$\{\Omega\} = \omega_0\{\ell_c\} + \{\Omega_I\} \quad (2)$$

where $\{\ell_c\}$ is the matrix of direction cosines between a unit vector along a_3 and the xyz axis system and is a function of $\theta_i (i=1,2,3,)$, ω_0 is the orbital rate, and the components of $\{\Omega_1\}$ are linear combinations of the θ_i $(i=1,2,3)$. For this non-natural system the Hamiltonian has the form

$$H = T_2 - T_0 + V_G + V_{EL} \quad (3)$$

where V_G and V_{EL} are the gravitational and elastic potential energies, and the terms T_2 and T_0 are kinetic energy terms. Specifically, the T_2 terms are quadratic in and the T_0 terms, independent of, generalized velocities. Note that T_R contributes to T_0.

In Ref. 6 it is shown that the stability of an equilibrium solution to the system differential equations is determined by the sign definiteness of the Hamiltonian. Testing the Hamiltonian for sign definiteness is difficult, due to the presence of spatial derivatives of the elastic displacements in V_{EL}. The bounding properties of Rayleighs quotient and the fact that T_2 is positive definite are used in Ref. 6 to show that stability is determined by testing the sign definiteness of

$$\kappa_2 = V_G - T_0 + \tfrac{1}{2}\sum_{i=1}^{n} \int_{Di} \rho_i \{u_{ci}\}^T [\Lambda_{1i}^2] \{u_{ci}\} dD_i \quad (4)$$

where $\{u_{ci}\}$ is the elastic displacement vector, $[\Lambda_{1i}^2]$ is a diagonal matrix of the squares of first natural frequencies associated with the various elastic displacements, and the ρ_i are the mass densities. Specifically, the equilibrium is stable if κ_2 is positive definite. Furthermore, the equilibrium is asymptotically stable is pervasive damping exists.

Illustrative Example

We shall be concerned with the stability of an Earth-pointing satellite consisting of a main rigid body with a flexible rod and a constant speed rotor attached (see Fig. 1). The rod coincides with the satellites principal axis z when in the undeformed state. In addition, the rotor is assumed to have its spin axis along the same axis.

The rods can undergo flexural motion in two orthogonal directions. The elastic deformaitons in these directions are denoted by u_1 and u_2 as shown in Fig. 1. For this example it will be assumed that the motion of the center of mass due to the elastic displacements is negligible. In addition, the rotor's spin relative to the xyz axes will be a constant, s. We shall be concerned with the stability of the equilibrium configuration in which the axes xyz and $a_1a_2a_3$ coincide. This equilibrium configuration is defined by $\theta_1 = \theta_2 = \theta_3 = u_1 = u_2 = 0$. It should be noted that this is not the only equilibrium position possible for this system.

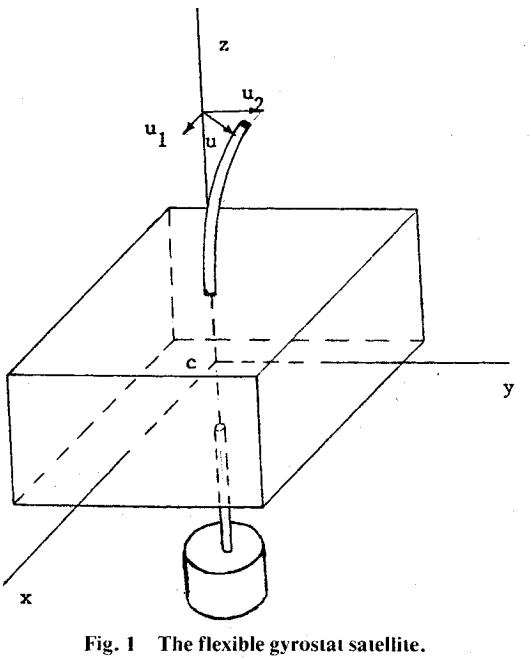

Fig. 1 The flexible gyrostat satellite.

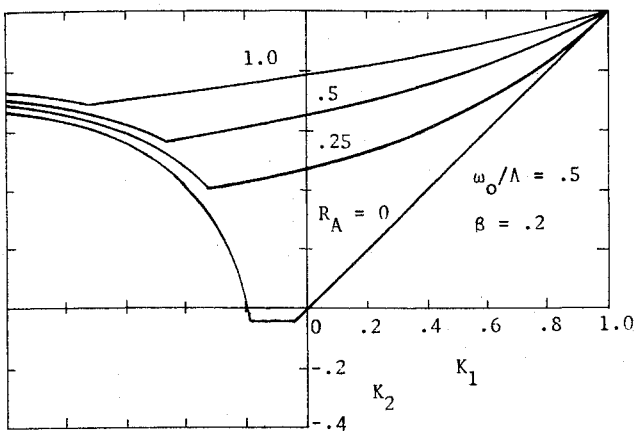

Fig. 2 Stability regions with R_A as a parameter.

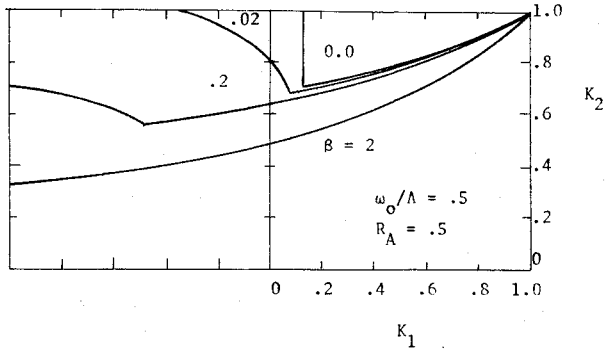

Fig. 3 Stability regions with β as a parameter.

In order to insure stability, κ_2 must be positive definite in the neighborhood of the equilibrium. Expanding κ_2 about the equilibrium and ignoring terms of order higher than two we obtain

$$\kappa_2|_E = \tfrac{1}{2}\omega_0^2\{(C-B)\theta_1^2 + (s/\omega_0)J\,\theta_1^2 + 4(C-A)\theta_2^2 + (s/\omega_0)J\,\theta_2^2 + 3(B-A)\theta_3^2 - 2\theta_1\int_h^{h+\ell}\rho z u_2 dz - 8\,\theta_2\int_h^{h+\ell}\rho z u_1 dz + \int_h^{h+\ell}\rho[(\Lambda_{1u_1}/\omega_0)^2 - 3]\,u_1^2 dz + \int_h^{h+\ell}\rho(\Lambda_{1u_2}/\omega_0)^2 u_2^2 dz\} \quad (5)$$

where A,B,C are the principal moments of inertia about axes xyz of the entire satellite in the undeformed state. In addition, J represents the moment of inertia of the rotor about its spin axis and Λ_{1u_1} and Λ_{1u_2} are the first natural frequencies of vibration of motions u_1 and u_2, respectively.

Testing $\kappa_2|_E$ for definiteness is complicated by its functional dependence on $u_1(z,t)$ and $u_2(z,t)$. As was first suggested in Ref. 7, this problem can be circumvented by defining integral coordinates

$$\bar{u}_1(t) = \int_h^{h+\ell}\rho z u_1(z,t)dz, \qquad \bar{u}_2(t) = \int_h^{h+\ell}\rho z u_2(z,t)dz \quad (6)$$

Through use of Schwarz's inequality we find that

$$\int_h^{h+\ell}\rho u_1^2 dz \geq \bar{u}_1^2/I_1; \quad \int_{h+\ell}\rho u_2^2 dz \geq \bar{u}_2^2/I_1 \quad (7)$$

where

$$I_1 = \int_h^{h+\ell}\rho z^2 dz$$

represents the moment of inertia of the rod about a transverse axis through c. In view of inequalities (7), we may define a function $\kappa_3 \leq \kappa_2|_E$ given by

$$\kappa_3 = \tfrac{1}{2}\omega_0^2\{[C-B+(s/\omega_0)J]\theta_1^2 + [4(C-A)+(s/\omega_0)J]\theta_2^2 + 3(B-A) - 2\theta_1\bar{u}_2 - 8\theta_2\bar{u}_1 + [(\Lambda_{1u_1}/\omega_0)^2 - 3]\bar{u}_1^2/I_1 + (\Lambda_{1u_2}/\omega_0)^2\bar{u}_2^2/I_1\}$$

If κ_3 is positive definite and pervasive damping exists, the null solution is asymptotically stable.

Using Sylvester's criterion, we find that κ_3 is positive definite if the following inequalities are satisfied:

$$K_1 + \beta(1-K_1K_2)/(1-K_2) - R_A(\omega_0/\Lambda_{1u_2})^2 > 0 \quad (9a)$$

$$K_2 + \beta(1-K_1K_2)/4(1-K_1) - 4R_A(1-K_2)/\cdot(1-K_1)[(\Lambda_{1u_1}/\omega_0)^2 - 3] > 0 \quad (9b)$$

$$K_2 - K_1 > 0 \quad (9c)$$

$$(\Lambda_{1u_1}/\omega_0)^2 - 3 > 0 \quad (9d)$$

where the parameters K_1, K_2, β, and R_A are given by

$$K_1 = (C-B)/A, \qquad K_2 = (C-A)/B \quad (10)$$

$$\beta = Js/C\omega_0, \qquad R_A = I_1/A \quad (11)$$

We note that these parameters are the same as used in Ref. 8 except for a change in the sign of K_2. Inequalities (9) represent sufficient conditions for stability in terms of the parameters $K_1, K_2, \beta, R_A, \Lambda_{1u_2}/\omega_0$ and Λ_{1u_1}/ω_0.

Numerical Results

In order to simplify the presentation of the results, the flexible rod is assumed to be uniform such that $\Lambda_{1u_1} = \Lambda_{1u_2} = \Lambda$. This assumption reduces by one the number of parameters involved in the problem. Figure 2 shows the regions of stability in the parameter plane defined by K_1 and K_2 for fixed values β and ω_0/Λ for various values of R_A. the region above each curve is stable. In the absence of the flexible rod, i.e., when $R_A = 0$, the satellite becomes totally rigid and the plot reduces to that of Ref. 8. As the inertia of the rod increases, i.e., as R_A increases in value, the stable region decreases, which is to be expected. Figure 3 shows the effect of varying the parameter β while holding ω_0/Λ and R_A fixed. The stable regions increase in size for increasing values of β. Reference 9 considers the problem of a gravity-stabilized satellite with six appendages. The results presented here agree with those of Ref. 9 exactly when $\beta = 0$.

Conclusions

The problem of altitude stability of a gravity-stabilized satellite with internal rotors and flexible appendages has been formulated and an example solved. Through use of the method of integral coordinates in conjunction with a Liapunov stability analysis, closed-from stability criteria were obtained. As expected, the results reduce to those of Ref. 8 if the rods are assumed rigid and to those of Ref. 9 if the internal rotors are ignored. Since the results obtained represent only sufficient conditions, any errors in predicting possible instabilities are on the safe side.

References

[1] Meirovitch, L. and Nelson, H.D., "On the High Spin Motion of a Satellite Containing Elastic Parts," *Journal of Spacecraft and Rockets*, Vol. 3, Nov. 1966, pp. 1597-1602.

[2] Robe, T.R. and Kane, T.R., "Dynamics of an Elastic Satellite – Parts I, II and III," *International Journal of Solids and Structures*, Vol. 3, 1967, pp. 333-352, 691-703, 1031-1051.

[3]Dokuchaev, L.V., "Plotting the Regions of Stable Rotaiton of a Space Vehicle with Elastic Rods," *Kosmicheskic Issledovdniya* (English Translation), Vol. 7, July-Aug. 1969, pp. 534-546.

[4]Brown, D.P. and Schlack, A.L., "Stability of a Spinning Body Containing an Elastic Membrane via Liapunov's Direct Method," *AIAA Journal*, Vol. 10, Oct. 1972, pp. 1286-1290.

[5]Levinson, D. and Kane, T.R., "Spin Stability of a Satellite Equipped with Four Booms," *Journa. of Spacecraft and Rockets*, to be published.

[6]Meirovitch, L., "Liapunov Stability Analysis of Hybrid Dynamical Systems with Multi-Elastic Domains," *International Journal of Non-Linear Mechanics*, Vol. 7, 1972, pp. 425-443.

[7]Meirovitch, L. and Calico, R., "The Stability of Motion of Force-Free Spinning Satellites with Flexible Appendages," *Journal of Spacecraft and Rockets*, Vol. 9, April 1972, pp. 237-245.

[8]Crespo Da Silva, M.R.M., "Attitude Stability of a Gravity-Stabilized Gyrostat Satellite," *Celestial Mechanics*, Vol. 2, 1970, pp. 147-165.

[9]Merovitch, L. and Calico, R.A., "A Comparative Study of Stability Methods for Flexible Satellites," *AIAA Journal*, Vol. 11, Jan. 1973, pp. 91-98.

Effect of Mass Addition on the Boundary Layer of a Hemisphere at Mach 6

A. Demetriades,* A. J. Laderman,† L. Von Seggern,‡
Aeronutronic Ford Corporation, Newport Beach, Calif.

A. T. Hopkins,§
SAMSO/RSSE, Los Angeles, Calif.

and

J. C. Donaldson¶
ARO, Inc., Tullahoma, Tenn.

Nomenclature

A = surface area
D = diameter of hemispherical tip
f_w = nondimensional injection mass-flux
M = constant in the mass-flux distribution [Eq. (1)]
$\dot{M}$ = total mass injected through hemisphere (mass per unit time)
$\dot{m}$ = local mass flux (mass per unit area and time)
N = constant in the mass-flux distribution [Eq. (1)]
p_c = hemisphere internal pressure
Re_{D_∞} = $\rho_\infty u_\infty D/\mu_\infty$
Re_θ = local momentum Reynolds number
S = constant determined from the data [Eq. (2)]
u = velocity parallel to model axis (or surface)
v = velocity normal to model surface
β = local pressure gradient
δ = boundary-layer thickness
μ = viscosity
ρ = density
φ = angle measured from stagnation point
$( )_e$ = at boundary-layer edge
$( )_T$ = at boundary-layer transition
$( )_w$ = wall properties
$( )_\infty$ = freestream properties

Received Jan. 20, 1976; revision received March 31, 1976. Work supported by USAF/SAMSO under Contract F04701-71-C-0035.

Index categories: Boundary Layers and Convective Heat Transfer—Laminar; Boundary-Layer Stability and Transition.

*Supervisor, Fluid Mechanics Section. Associate Fellow AIAA.
†Principal Scientist. Member AIAA.
‡Engineer.
§Project Engineer, Lieutenant, USAF.
¶Project Engineer.

CONSIDERABLE theoretical work has been performed to examine boundary-layer development on blunt bodies at hypersonic speeds and the associated heat transfer with both passive-ablator and active-transpiration cooled materials. Direct experimental data, on the other hand, are scarce on the blunt body laminar boundary layer and on the conditions which cause transition to turbulence. This scarcity is, of course, due mainly to the obvious difficulties of probing the boundary layer near stagnation points. This Note presents boundary-layer development and transition results for a smooth spherically blunted cone with essentially zero heat transfer but with finite mass transfer rates.

The experiment was conducted in the 50-in. diameter Hypersonic Wind Tunnel B of the Arnold Engineering and Development Center (AEDC). A spherically blunted 5-deg half-angle cone with a 7-in.. nose radius was operated adiabatically at a nominal Mach 6 continuous flow condition. The stagnation temperature was 390° F and supply pressures ranged from 160 to 280 psia ($3.86\times10^6 < Re_{D\infty} < 6.18\times10^6$). The spherical nose was built of porous sintered stainless steel with an effective permeability of 0.94×10^{-9}cm^{-2}, and was designed with a variable wall thickness to allow gas injection when its interior was pressurized. (Pressures, p_c, ranging up to 35 psia were used.) The resultant surface mass flux distribution was

$$\dot{m}(\varphi) = M\cos 2\varphi + N \tag{1}$$

so as to simulate the mass flux distribution on an ablating reentry body. In the present case the injectant was air at near-stagnation temperature. Typical values of M and N, for example at $p_c = 19.7$ psia, were 0.00675 and 0.00875 lb/ft^2 sec respectively.

For $\varphi > 40°$, the flow was surveyed by external probes lowered to the surface through the tunnel ceiling. At $\varphi = 10°$, 20° and 30°, probes were extended and retracted at will from the inside of the model, through 0.035″ diam holes on its surface. The internally actuated probes were either 0.002″ diam (etched down from 0.004″ diam tubing) and 0.010″ diam pitot probes or 0.00002″ diam hot wire anemometers. A complement of surface pressure taps, thermocouples, heat transfer gages, acoustic sensors and accelerometers was installed to provide additional flow data and to monitor the model behavior.

The boundary-layer profiles shown in Fig. 1 were derived from the pitot measurements assuming a constant-pressure layer with a linear total temperature change from the layer edge to the surface. Corresponding theoretical laminar flow profiles (Fig. 1) have been supplied by Bywater.[1] The agreement is judged adequate, especially if one considers the marginal resolution of the pitot probe at $\varphi < 30°$, where the boundary-layer thickness was no more than 10 times larger than the probe diameter. Similarly, the measured boundary-

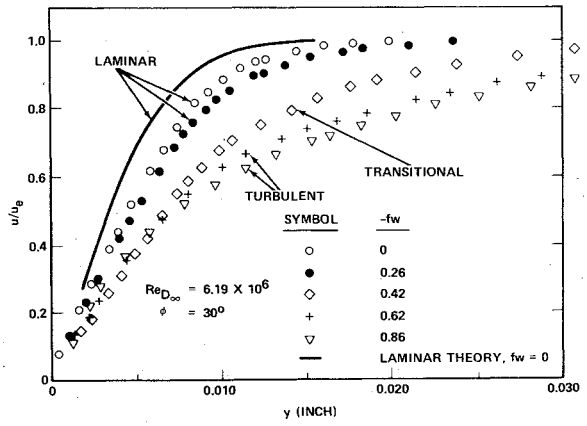

Fig. 1 Boundary-layer velocity profiles for various mass injection rates.